Solvent Magnetization Artifacts in High-Field NMR Studies of Macromolecular Hydration

Alexander G. Sobol,[1] Gerhard Wider, Hideo Iwai, and Kurt Wüthrich

Institute for Molecular Biology and Biophysics, ETH-Hönggerberg, CH-8093 Zürich, Switzerland

With the use of high magnetic fields and improved quality factor ratings of the probeheads in modern NMR spectrometers, radiation damping becomes more and more important. In addition, the demagnetizing field effect from protonated solvents gains significance with the increase of the magnetic field strength. During a typical NMR pulse sequence the magnetic fields caused by these effects become time-dependent, which makes the system nonlinear and may, for example, measurably influence the precession frequencies of all nuclei in the sample. Since radiation damping can affect signals that are several kilohertz away from the solvent resonance, the amplitude, phase, and frequency of the desired signals can be disturbed so as to give rise to spectral artifacts. In particular when difference methods are used to obtain the final spectrum, the data sets may be severely deteriorated by such artifacts. This paper investigates effects from the demagnetizing field and from radiation damping with a selection of pulse sequences in use for studies of macromolecular hydration, and strategies are described for the detection and elimination of the ensuing artifacts. © 1998 Academic Press

Key Words: **radiation damping; demagnetizing field; protein hydration; nucleic acid hydration.**

INTRODUCTION

Radiation damping is a well-known effect in high-resolution solution NMR, in which solvent magnetization is rotated back to the external magnetic field direction by the strong coupling of the magnetization with the resonant circuit of the detection system (*1*). Radiation damping complicates selective excitation of solvent resonances (e.g., Ref. *2*) and solvent signal suppression (e.g., Ref. *3*). The effect becomes more and more important at higher static magnetic field strengths and with improvements in the probe quality factors *Q*. Radiation damping is commonly assumed to affect signals only in a narrow frequency range close to the solvent resonance. Here, we demonstrate that radiation damping can influence signals with resonance frequencies differing by

several kilohertz from that of the solvent signal. These effects need to be taken into account whenever an experiment uses neither active electronic feedback (*4, 5*) nor variable *Q*-switching (*6*) to suppress radiation damping.

The demagnetizing field in an NMR sample is caused mainly by highly abundant species, such as the solvent, and was for many years considered to be a phenomenon of little practical importance for NMR (*7*). The terms ''dipolar field'' (e.g., Ref. *8*) and ''bulk susceptibility effect'' (e.g., Ref. *9*) are alternatively used to denote the same effect. Nonlinear behavior due to the nuclear demagnetizing field was observed first for solid ^{3}He (*10*) and later on for liquid ^{3}He (*11*). It was predicted that similar effects should be observable for water at room temperature at magnetic field strengths higher than 1 T (*10*). Indeed, numerous manifestations of the demagnetizing field effect in liquid-state NMR were reported during the past few years. For pulsed experiments, transient changes in the magnetic field due to nuclear magnetization of the solvent were observed (*9*), and multiple spin echoes in liquids at high magnetic fields were reported to originate from the demagnetizing field (*12–14*). An explanation of ''impossible'' cross peaks between solvent and solute molecules in terms of multiple-quantum coherences (*15–17*) was recently a subject of controversy (*8, 18–21*). Several applications were proposed which make use of intrinsic features of NMR in the presence of the demagnetizing field for indirect detection of one spin species in a NMR sample via the NMR signal of another species (*22, 23*) and for measuring self-diffusion in liquids (*24*), and it was pointed out that optimal solvent signal suppression could be achieved only if the demagnetizing field effect was adequately accounted for (*25, 26*).

Investigation of the hydration of biological macromolecules in solution is an attractive application of NMR spectroscopy in structural biology (e.g., Refs. *27–32*). NMR pulse sequences for hydration studies must be laid out for the detection of weak signals in the presence of very intense solvent lines, which has been achieved with the use of selective excitation techniques, with exploitation of radiation damping, with the use of isotope filtering, differential diffu-

sion, or differential relaxation properties (*33–41*). In most cases, the NMR experiments for studies of macromolecular hydration make use of difference techniques, and are therefore particularly prone to deterioration by artifacts originating from specific NMR properties of the solvent, such as radiation damping and the nuclear demagnetizing field. This paper demonstrates the presence of such artifacts in 750-MHz experiments with a selection of experimental schemes for studies of hydration. Strategies are then developed for the elimination of these unwanted signals.

MATERIALS AND METHODS

All NMR data were acquired on a Varian 750 UNITY-Plus spectrometer operating at a ^{1}H resonance frequency of 750 MHz.

^{31}P NMR

We recorded ^{31}P spectra of 100 mM NaH$_2$PO$_4$ in 90% H$_2$O/10% D$_2$O to demonstrate the effect of the proton demagnetizing field and to evaluate the lock system response. Radiation damping was reduced by using a sample volume of 150 μl in a ''heavy-wall'' NMR tube with only 2-mm inner diameter. The time domain data ($s(t)$) were transformed to polar coordinates:

$$M(t) = \sqrt{\mathrm{Re}(s(t))^2 + \mathrm{Im}(s(t))^2},$$

$$\varphi(t) = \mathrm{Arctan}\,\frac{\mathrm{Im}(s(t))}{\mathrm{Re}(s(t))}. \quad [1]$$

The signal amplitude, $M(t)$, represents the transverse component of the magnetization and hence contains information on spin–spin relaxation, whereas the phase of the signal, $\varphi(t)$, carries detailed information on field changes.

Pulse Sequences

The pulse sequences used to investigate the influence of radiation damping and the demagnetizing field effect on hydration studies are presented in Fig. 1. In Fig. 1A, which derives from a scheme described previously (*40*), the first scan uses radiation damping to rotate the water magnetization back to the equilibrium direction after the 90° pulse that follows the relaxation period τ_{rel}, and prior to the heteronuclear relay step, {^{15}N,^{1}H}-HSQC, all transverse magnetization is dephased by the gradient G_2. In the second scan, all transverse magnetization is dephased immediately after the 90° pulse by the gradient, G_2 in g_z(II), which prevents radiation damping. The difference spectrum obtained from these two scans contains water–protein NOEs, exchange peaks with water, and possibly HN–C$^\alpha$H NOEs when C$^\alpha$H chemical shifts are close to that of water. For long mixing times some spin diffusion peaks may be present as well.

Figure 1B represents a pulse sequence that uses radiation damping as described in Ref. (*38*), and which is supplemented with a {^{15}N,^{1}H}-HSQC relay step. The pulse sequence in Fig. 1C derives from Ref. (*34*) and was implemented as in the original publication, except that the original 1-ms rectangular water flip-back pulse in the {^{15}N,^{1}H}-HSQC relay step was replaced by a 2-ms pulse with the shape of the center lobe of a sinc function, which ensures more satisfactory difference spectra in the solvent presaturation test described below. Modifications of the gradient sequence represented with broken lines were used in some recordings to reduce radiation damping effects. To prevent artifacts originating from non-steady-state conditions, all pulse schemes start with the sequence G_1–90° (^{1}H)–G_1 to dephase all proton magnetization.

Test Procedures

Hydration measurements require utmost stability of the spectrometer and robustness of the pulse sequence. To check on the suitability of the pulse sequences in Fig. 1 for the intended purpose, we devised a series of stringent test measurements.

To obtain artifact-free difference spectra, perfect subtraction of the signals must be achieved in the relay step alone, i.e., {^{15}N,^{1}H}-HSQC in the experiments of Fig. 1. Perfect cancellation for the relay step documents that the stability of the spectrometer is sufficient, the magnetic field gradients used do not create artifacts, the parameters of the field–frequency lock system (such as the lock time constant) have been set properly, and possible small differences in the implementation of the relay step for the two recordings I and II (see Fig. 1) (for example, in the phase of the water flip-back pulse) do not interfere with proper performance.

Solvent presaturation must result in a spectrum which contains no solvent proton–macromolecular proton NOEs. This test is necessary but not sufficient to ensure artifact-free experiments, since the dipolar field and the radiation damping effects are also suppressed by the presaturation. For some pulse sequences slight modifications of the test procedure may be required (*42*).

In a difference spectrum obtained with a very short mixing time only exchange peaks should be detectable. This was checked by inspection of the signal buildup in a series of difference experiments recorded with increasing mixing times.

For the preliminary setup we used one-dimensional versions of these tests experiments, and before collecting the data of interest we recorded two-dimensional versions of the difference spectra with solvent presaturation or with very short mixing times.

NMR Samples

A 5 mM sample of a ^{15}N-labeled mutant form of the N-terminal 63-residue fragment of the 434-repressor, 434(1–
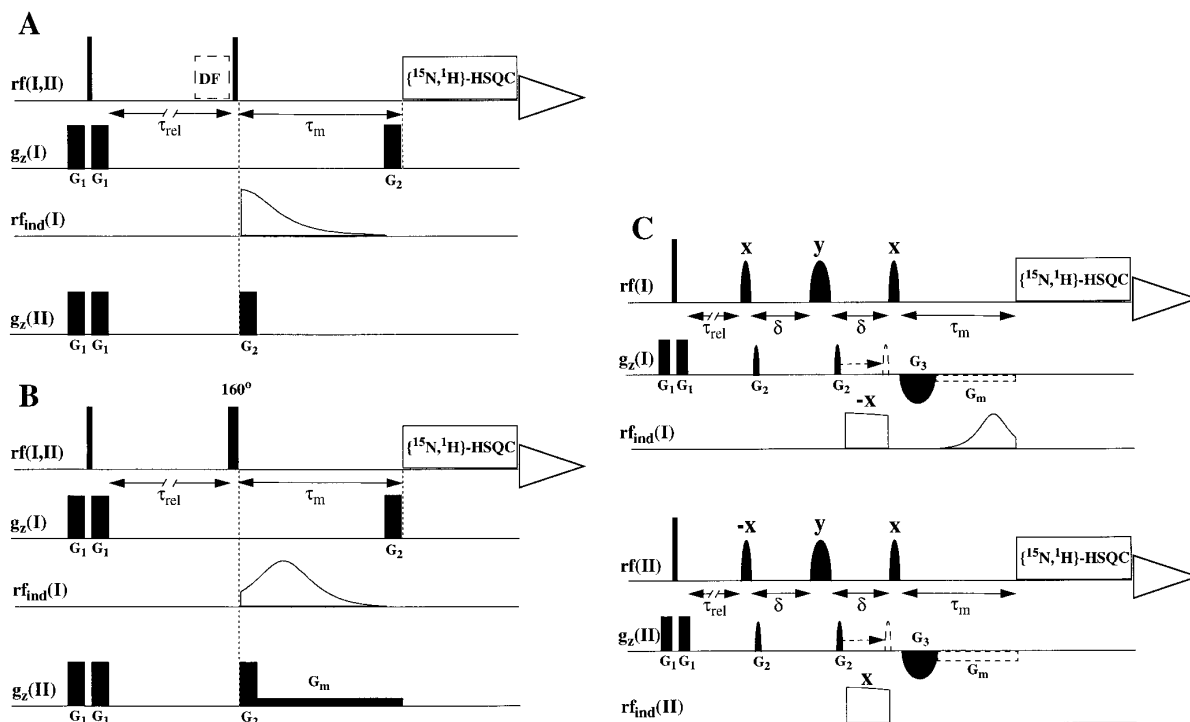
FIG. 1. Schematic representation of three 2D { ^{15}N, ^{1}H }-HSQC-relayed NOE difference experiments derived from previously published pulse sequences for protein hydration studies (34, 38, 40), which were used to investigate the influence of radiation damping. White boxes represent the relay step { ^{15}N, ^{1}H }-HSQC. For the schemes (A) and (B) the { ^{15}N, ^{1}H }-HSQC relay step was performed with sensitivity enhancement (53) and water flip-back (54). In scheme (C) the { ^{15}N, ^{1}H }-HSQC relay step was performed as described in the original publication of this experiment (34). In each experiment, I and II denote the two experimental schemes used to obtain the raw data from which the difference spectra were computed. On the rf line, narrow vertical bars stand for hard 90° proton pulses, broader bars stand for longer pulses as indicated, curved black shapes present selective pulses at the water frequency, and the box outlined by a broken line, DF, represents a ^{15}N double filter used for artifact suppression. Unless indicated otherwise, the pulses are applied with x phase. On the line g_z, black rectangles represent gradient pulses, curved black shapes indicate sine-bell-shaped gradients, and rectangles and curved shapes drawn with broken lines represent modifications of the pulse sequence that were introduced in some recordings to reduce radiation damping effects. On the line rf$_{ind}$, the radiofrequency induced by the coupling of the solvent magnetization with the receiving circuit is indicated. In (A) and (B) the line rf$_{ind}$(II) is not shown, since radiation damping is suppressed by G_2 in trace II. For all experiments the duration of the gradients G_1 was 2 ms, their strength was 32 G/cm, and the relaxation delay, τ_{rel}, was set to 2.5 s. In (A) and (B) the duration of the gradients G_2 was 2 ms and their strength was 30 G/cm; G_m in (B) was 0.5 G/cm. In (C) the radiofrequency pulses on the ^{13}C channel, which are an integral part of the experiment (34), are not shown. The proton pulses in the traces rf(I) and rf(II) are shaped with a center lobe of a sinc function and have a duration of 2 ms for a 90° pulse. The maximum strength of all the sine-bell-shaped gradients was 25 G/cm, with a duration of 0.5 ms for G_2 and 10 ms for G_3. The delay δ had a length of 2.4 ms.

63), was used to record spectra with the pulse schemes presented in Figs. 1A and 1B. The mutant protein has been shown to fold into a globular structure closely similar to that of the wild-type protein (H. Iwai and K. Wüthrich, in preparation). A 550-μl sample was buffered with 25 mM potassium phosphate in 90% H_2O/10% D_2O at pH 4.8 and measured at 13°C. For experiments with the pulse scheme in Fig. 1C, similar conditions were used, but the protein was ^{15}N, ^{13}C-doubly labeled and the concentration was 3 mM.

Simulation of Artifacts

Simulations of magnetization trajectories were performed by numerical solution of modified nonlinear Bloch equations that include terms describing radiation damping and the demagnetizing field (10, 43). Neither possible differences in

the spatial distributions of radiation damping and of the demagnetizing field in the sample nor possible effects from diffusion were considered in the simulations.

RESULTS AND DISCUSSION

Demagnetizing Field Effects

The magnetic field in a NMR sample is usually assumed to be constant during a NMR experiment. In reality, time-dependent fields, as represented schematically in Fig. 2, cause nonlinear behavior of the system. Edzes (9) showed that due to variations of the longitudinal component of the solvent magnetization small changes of the magnetic field may occur during pulse sequences. The longitudinal component of the demagnetizing field, $\mathbf{B}_{dz}$, affects all spins in a
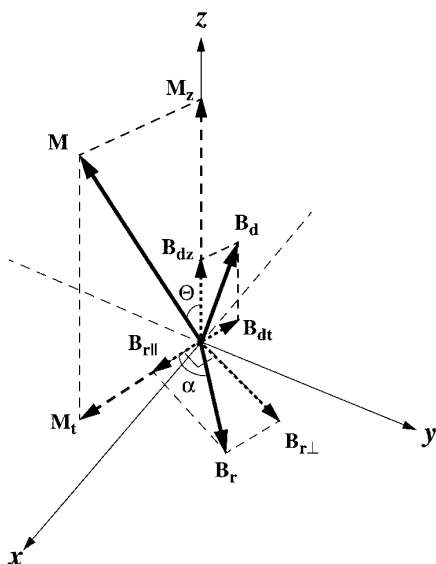
FIG. 2. Schematic representation of the demagnetizing field $\mathbf{B_d}$ and the radiation damping field $\mathbf{B_r}$ which originate from the magnetization $\mathbf{M}$ for a cylindrical sample of ''infinite'' length. $\mathbf{M}_z$ and $\mathbf{B}_{dz}$ denote the longitudinal components of $\mathbf{M}$ and $\mathbf{B_d}$, respectively. $\mathbf{M_t}$ and $\mathbf{B}_{dt}$ stand for the corresponding transverse components. The phase of the radiation damping, α, is in general different from $\pi/2$ (see text). $\mathbf{B}_{r\parallel}$ is the projection of $\mathbf{B_r}$ on $\mathbf{M_t}$, and $\mathbf{B}_{r\perp}$ is the component orthogonal to $\mathbf{M_t}$.

macroscopic sample. Relaxation and radiation damping lead to time variations of the magnetic field during the evolution period, which results in frequency variations that cause distorted lineshapes. Such effects can best be studied using the time domain data of a sample with a one-line spectrum that is placed in a highly homogeneous field. We analyzed the FID of the ^{31}P line of NaH$_2$PO$_4$ dissolved in 90% H$_2$O/10% D$_2$O in polar coordinates represented by the magnetization $M(t)$ and the phase $\varphi(t)$ (see Materials and Methods), where $\varphi(t)$ carries detailed information on field changes. Figure 3A shows the time variations in the phosphorous precession frequency, represented by $\varphi(t)$, as a function of the length of a proton pulse, β, that precedes the $90°(^{31}\text{P})$ pulse before ^{31}P acquisition. For $\beta = 0°$ the phosphorous signal is set on resonance, so that the initial slope of the plot $\varphi(t)$ versus the acquisition time reflects the change of the phosphorous precession frequency ($\frac{d\varphi}{dt} \times \frac{1}{2\pi}$) and, hence, the change of the effective magnetic field caused by the proton pulse β. A maximal effect of 0.6 Hz on the precession frequency was observed for $\beta = 180°$, as compared to the theoretical estimate of 0.76 Hz for a cylindrical sample (9). If the actual experimental coil and sample geometries were taken into account, the theoretical estimate would also be smaller than 0.76 Hz. Radiation damping and longitudinal relaxation of the solvent change the dipolar field effect during acquisition, and therefore the plots of $\varphi(t)$ versus the acquisition time are not linear.

The experiment of Fig. 3A was performed without field–frequency lock during acquisition. Since all nuclei in the sample, including deuterium, are exposed to the same time variation of the magnetic field, one can expect that a ^{2}H field–frequency lock might partially compensate for the longitudinal component of the induced field changes. Thereby the response to nearly instantaneous changes of the magnetic field strongly depends on the time constant of the lock system. Figure 3B shows the dependence on the time constant of the lock system efficiency in compensating for the demagnetizing field after a $180°(^1\text{H})$ pulse. For sufficiently short time constants and concomitant fast lock response, one can obtain significant suppression of the effect.

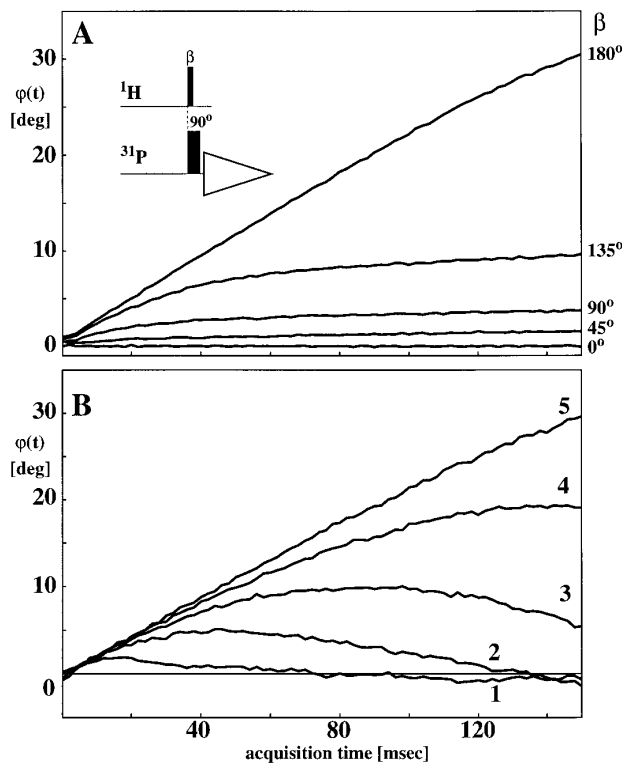The demagnetizing field also has a transverse component,

FIG. 3. Demonstration of the demagnetizing field effect and the efficiency of a field–frequency lock with variable lock time constant, using 1D ^{31}P NMR of 100 mM NaH$_2$PO$_4$ in 90% H$_2$O/10% D$_2$O. The pulse sequence used is shown as an inset in (A). Equation [1] was used to calculate the signal phase, $\varphi(t)$, as a function of the acquisition time. (A) Time evolution of $\varphi(t)$ for the phosphorous signal during acquisition without field–frequency lock when applying a proton pulse with variable flip angle, β, prior to detection. The offset was chosen so that the phosphorous signal was on resonance for $\beta = 0°$. (B) Time evolution of $\varphi(t)$ for the phosphorous signal during acquisition in experiments with $\beta = 180°$ and different settings of the lock time constant. Curve 5 was obtained without lock and corresponds to the curve for $\beta = 180°$ in (A). The curves 4, 3, 2, and 1 were recorded with decreasing values of the lock time constant (Vnmr parameter lockacqtc = 4, 3, 2, and 1, respectively), resulting in a faster response of the lock system to disturbances. The difference in noise amplitude between (A) and (B) is due to the fact that different numbers of scans were accumulated in the two types of experiments.

B$_{dt}$, (Fig. 2) (*20*). The effect of the transverse component vanishes with increasing frequency offset from the solvent. Consequently, even an ideal lock system cannot fully compensate for the demagnetizing field effect on the solvent and on signals within several kilohertz of the solvent resonance. Since it originates from the solvent magnetization, the transverse component of the demagnetizing field produces a solvent frequency shift (e.g., Refs. *20, 44*), and it cannot change the longitudinal component of the solvent magnetization. The demagnetizing field depends strongly on the sample geometry and would vanish completely in a spherical sample (e.g., Ref. *9*), but the use of a spherical sample is not practical as it results in a dramatically reduced filling factor. If the solvent magnetization is in different ''states'' during the evolution periods of the two data sets to be subtracted, a difference NMR spectrum will contain ''dispersive-like'' (''antiphase-like'') artifacts (*9*), which are especially pronounced for narrow signals. Because phase cycling is a type of subtraction procedure, it alone can already produce such artifacts (e.g., Ref. *45*).

Radiation Damping Effects

Radiation damping is the result of interactions between the magnetization vector and the resonant electric circuit, which can be represented as an induced shaped radiofrequency pulse. For periods of free evolution the shape of such pulses is reminiscent of a hyperbolic secant (*1*). For example, if the angle between the solvent magnetization and the magnetic field at the beginning of an evolution period is Θ (see Fig. 2), then the amplitude of the radiation damping field is given by (e.g., Refs. *44, 46*)

$$|\mathbf{B}_r(t)| = A \cdot \mathrm{sech}\left\{\frac{t}{\tau_r} - \ln\left(\tan\frac{\Theta}{2}\right)\right\}, \qquad [2]$$

where A is the maximum strength of the radiation damping field, and τ_r is a damping time constant which depends on the magnitude of the solvent magnetization, the gyromagnetic ratio, the quality factor of the probehead, and the filling factor of the coil. Equation [2] does not account for solvent relaxation. If the probe is perfectly tuned to the solvent frequency, then the radiation damping field lags behind the solvent magnetization by 90° (in Fig. 2, $\alpha = 90°$ and $|\mathbf{B}_{r\parallel}| = 0$) (*43*). Slight detuning of the receiving circuit to a frequency different from the solvent resonance (providing that the resonance width of the probe is large compared to this difference) leads to a small change in the phase of the radiation damping field $\mathbf{B}_r$, α, and $\mathbf{B}_{r\parallel}$ does not vanish any more (Fig. 2). The effect of the transverse demagnetizing field $\mathbf{B}_{dt}$ mentioned above is thus equivalent to the effect of $\mathbf{B}_{r\parallel}$ which may result from a small phase shift of the radiation damping field (*44*) (Fig. 2). In principle, therefore, probe detuning can be used to reduce the effect of the transverse

component of the demagnetizing field by fulfilling the condition $\mathbf{B}_{r\parallel} = -\mathbf{B}_{dt}$ (Fig. 2).

Consequences of Radiation Damping and the Demagnetizing Field Effect for Studies of Macromolecular Hydration

Manifestations of radiation damping for a particular pulse sequence can be simulated on the basis of modified Bloch equations (e.g., Ref. *44*). For simplicity of the presentation we restrict the following considerations to radiation damping during periods of free evolution, without accounting for relaxation. An evolution period with radiation damping can then be represented by a properly shaped pulse, i.e., a truncated hyperbolic secant pulse (see Eq. [2], where Θ is predefined by the pulse sequence used, A and τ_r must be determined experimentally, and the truncation (see Fig. 1) is dictated by the available free evolution time). Such a pulse may disturb the magnetization of spins that resonate as much as several kilohertz away from the solvent signal. We used this simplified formalism to examine the consequences of radiation damping for studies of solvent–macromolecule NOEs. In the difference techniques used for solvent–solute NOE measurements shown in Fig. 1, radiation damping is included in the form of ''induced'' shaped rf pulses to indicate periods where small differences between the scans I and II may result. Figure 4 shows spectra obtained with the pulse sequences of Fig. 1 for a mutant form of the N-terminal domain of the 434-repressor, 434(1–63). A spectrum obtained with the experiment where radiation damping is represented by a $\mathrm{sech}(t/\tau_r)$-shaped pulse according to Eq. [2] (Fig. 1A) contains signals for all amide protons in the protein except one, the position of which is indicated by a circle (Fig. 4A). Such a result can hardly be expected for a globular protein with a well-defined core that protects part of the amide protons from solvent contact. A standard control 2D spectrum recorded with weak presaturation of the water resonance before the start of the actual pulse sequence was found to contain no peaks. To further investigate possible sources for the apparent artifactual peaks in Fig. 1A, several additional test were used as described in the following.

A series of 1D $\{^{15}N, {}^{1}H\}$-HSQC-relayed NOE difference spectra were recorded with variable τ_m to investigate the signal buildup. These spectra show strong offset-dependent oscillations for very short τ_m values. Figures 5A and 5C display such oscillations for two signals with offsets from the water resonance of 1506 and 2651 Hz, respectively. The oscillations originate from an offset-dependent effect of the radiation damping field ($\mathrm{sech}(t/\tau_r)$) on the transverse component of proton magnetization. They decay with increasing mixing time, τ_m, and have an envelope of $\mathrm{sech}(t/\tau_r)$, which is defined by the radiation damping, and reach asymptotically a nonzero, negative value (dashed lines in Fig. 5). Numerical results can be obtained by simulations (Figs. 5B
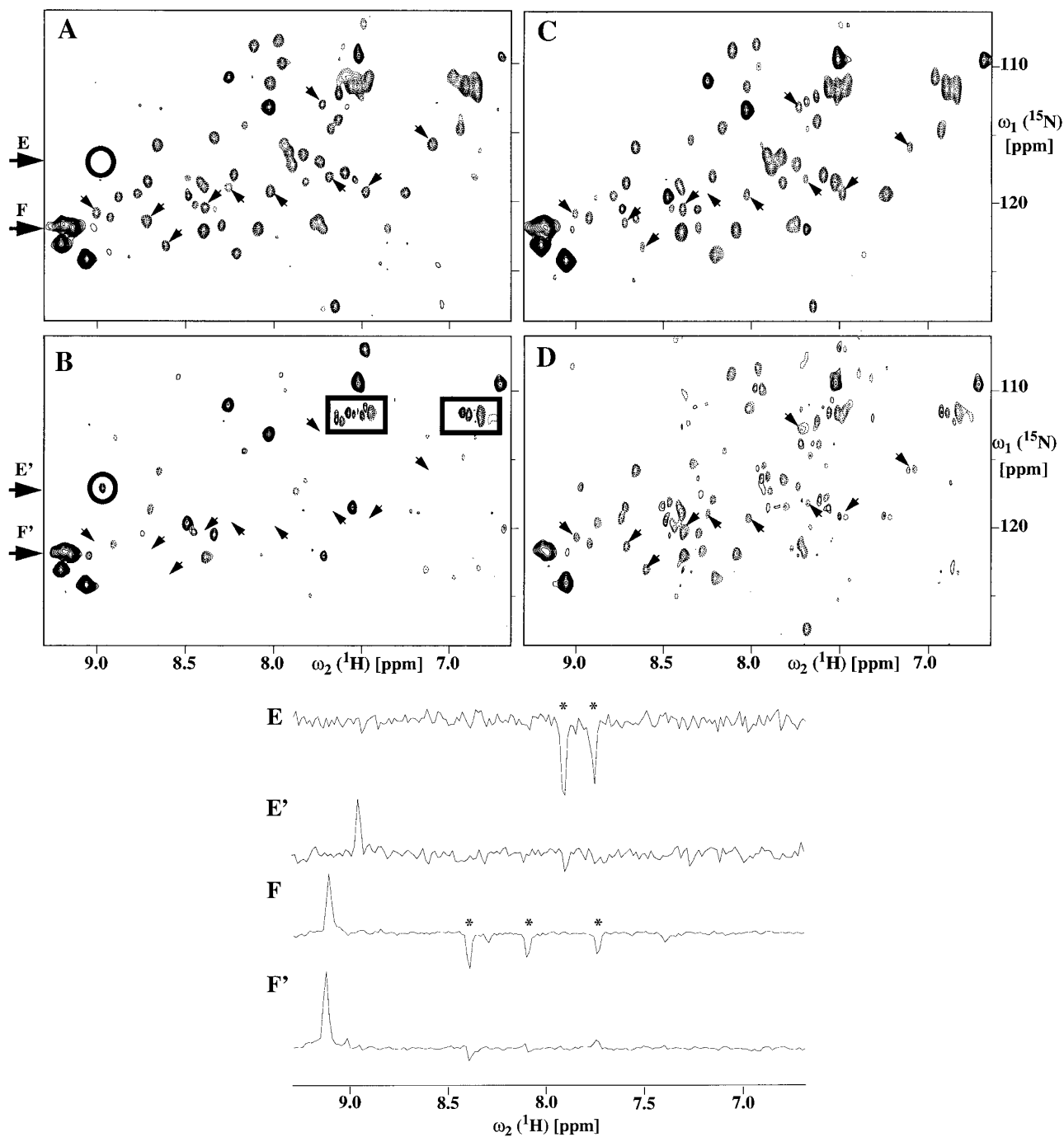
FIG. 4. (A)–(D) Contour plots of the spectral region (ω_1(^{15}N) = 106.0–128.5 ppm, ω_2(^{1}H) = 6.6–9.3 ppm) of 2D {^{15}N,^{1}H}-HSQC-relayed NOE difference experiments. In (A), (B), and (C) the sample used was a 5 mM solution of a uniformly ^{15}N-labeled mutant form of the 63-residue N-terminal DNA-binding domain of the 434, 434(1–63). For (D), a 3 mM ^{15}N,^{13}C-labeled sample of the same protein was used. For all four experiments the solvent was 90% H$_2$O/10% D$_2$O, pH 4.8 and T = 13°C. Positive peaks are drawn with solid lines and negative peaks with dashed lines. (A) Spectrum obtained with the sequence in Fig. 1A, using τ_m = 68 ms. The circle indicates the position of the only backbone amide signal that is missing when compared to the {^{15}N,^{1}H}-HSQC spectrum recorded with the same conditions. The arrows point to peaks that correspond to residues with less than 5% solvent accessibility. (B) Same as (A), except that a ^{15}N double filter was inserted into the pulse sequence (DF in Fig. 1A). Rectangles indicate subtraction artifacts originating from the demagnetizing field effect. (C) Spectrum obtained with the pulse sequence of Fig. 1B, with τ_m = 100 ms. (D) Spectrum obtained with the experiment of Fig. 1C, with τ_m = 60 ms. (E)–(F′) Two pairs of corresponding cross sections from the spectra (A) and (B), taken along ω_2(^{1}H) at the ω_1(^{15}N) chemical shifts indicated by the arrows in (A) and (B). The asterisks identify artifactual peaks in the traces E and F.
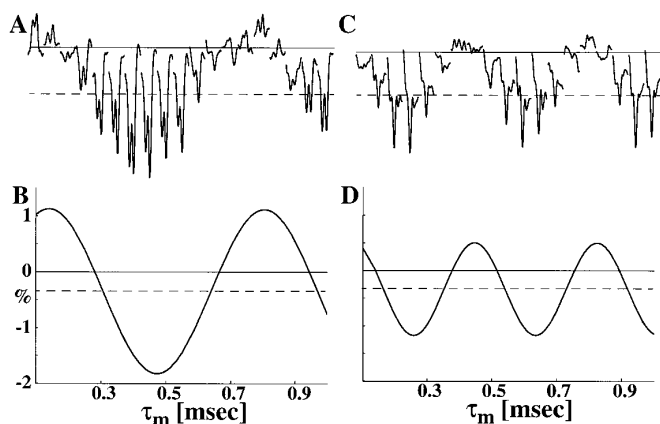
FIG. 5. Plots of the buildup from $\tau_m = 100$ μs to 1 ms of two signals in the experiment of Fig. 1A with offsets from the water resonance of 1506 Hz (A) and 2651 Hz (C). Panels (B) and (D) show simulations of the expected effect for these signals. Asymptotic values for the oscillations are indicated by dashed lines. The simulation was based on modified Bloch equations that take the influence of radiation damping and the demagnetizing field into account (44). Simulated intensities are given in percent of the equilibrium magnetization of the protein protons before the start of the pulse sequence.

and 5D) based on modified Bloch equations (44), taking into account the evolution of the magnetization during the 90° pulse (10.6 μs) and the following short delay (16.9 μs) before the start of the gradient G_2 (trace g_z(II) in Fig. 1A). There is a striking similarity between the measured and simulated data. The residual difference between the offsets of the oscillations in the experimental and simulated results (dashed lines in Fig. 5) is primarily due to differences in the radiation damping phase, which depends on the tuning of the probe. The nonvanishing offset gives rise to artifacts, i.e., negative peaks with intensities of the order of 1% of the equilibrium magnetization of the protein protons before the start of the pulse sequence. An additional modulation of the signal buildup by spin–spin coupling can be observed for longer mixing times, but the asymptotic behavior of the artifactual signals is not changed.

Currently used precautions for reducing adverse effects of radiation damping consist of using small sample volumes and keeping the solvent defocused by field gradients (e.g., Ref. 39), active electronic feedback (4, 5) (not commercially available), or Q-switching (6). Of course, these approaches cannot be used to suppress artifacts in pulse sequences based on selective water flip-back by radiation damping. In the experiment of Fig. 1A the artifacts can be eliminated by modifying the pulse sequence in such a way that there is no transverse magnetization during τ_m for all ^{15}N-bound protons. This can be achieved by the addition of a ^{15}N double filter, DF (47, 48), as indicated in Fig. 1A. The choice of the ^{15}N filter used is not critical. The only limitation is that solvent magnetization before and after the filter should not differ significantly, to prevent loss of sensi-

tivity. This can be verified by comparing the integral of the solvent signal before and after the filter in separate experiments. The modified experiment results in the spectrum shown in Fig. 4B. At the position indicated by a circle in Figs. 4A and 4B, there is now a weak positive exchange peak, which was apparently canceled in (A) by artifactual negative peak intensity. All peaks observed in the spectrum of Fig. 4B correspond to amide protons of amino acid residues that are either near the protein surface or have the H$^\alpha$ chemical shift close to the water resonance. Interior amide protons (arrows in Fig. 4) no longer show ''NOEs'' to water protons. To compare the relative amplitudes of artifactual and real signals, cross sections through the two data sets are shown in Figs. 4E, 4E′, 4F and 4F′.

Figure 4B still contains ''dispersive-like'' peaks (framed by the two rectangles) that originate from the effect of the demagnetizing field during acquisition. These peaks were masked by other strong artifacts in Fig. 4A. These dispersive-like peaks can be suppressed by omitting the water flip-back pulse in the {^{15}N,^{1}H}-HSQC relay step. Since the water magnetization at the end of the mixing period τ_m is either aligned along $+z$ (trace I of Fig. 1A) or dephased (trace II in Fig. 1A) in the two experiments to be subtracted, the use of the water flip-back pulse in the {^{15}N,^{1}H}-HSQC relay step results in slightly different magnetic fields in the sample during acquisition. The absence of a similar dispersive-like pattern in the ^{15}N dimension is explained mainly by the averaging of the demagnetizing field effect (e.g., Ref. 49) achieved by the proton 180° refocusing pulse in the middle of the ^{15}N evolution period, and the downscaling of the demagnetizing field effect by the coefficient of the gyromagnetic ratios. Dispersive-like artifacts in the direct and/or indirect dimensions have been observed for methyl lines and other sharp resonances in homonuclear and heteronuclear difference experiments (e.g., Ref. 50) and it seems very likely that artifacts similar to those in NOE experiments (Fig. 4B) will also be found in water–protein ROE experiments; they can usually be suppressed by minor modifications of the pulse sequence (e.g., Ref. 45).

The pulse sequence of Fig. 1B for the detection of solvent–macromolecular NOEs is based on selective water flip-back by radiation damping (38). In Fig. 1B the radiation damping after the 160° ^{1}H pulse is represented by a sech $(t/\tau_r - 1.74)$-shaped pulse (see Eq. [2]). A standard test spectrum acquired with presaturation of the water resonance before the start of the actual experiment contained no signals. Comparison of the spectrum obtained using the technique of Fig. 4C with the spectra in Figs. 4A and 4B shows that it contains artifactual peaks of significant amplitude. The origin of these artifacts is identical to that for the previously described pulse sequence of Fig. 1A, the only difference being that the amplitude of the oscillations is predefined by sech$(t/\tau_r - 1.74)$ and has a maximum at $t = 1.74$ τ_r. The pulse sequence of Fig. 1B is intrinsically more sensitive than
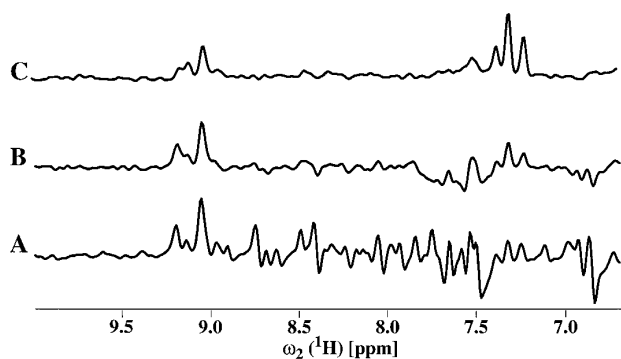
FIG. 6. Spectral region (6.6–10.0 ppm) in the first FID of three different {^{15}N,^{1}H}-HSQC-relayed NOE difference experiments measured with a 3 mM solution of ^{15}N,^{13}C-labeled mutant 434(1–63) in 90% H$_2$O/10% D$_2$O at pH 4.8 and 13°C. (A) Spectrum obtained with the experiment of Fig. 1C. (B) Same as (A), except that radiation damping effects were reduced by an additional gradient applied during the mixing time (G_m in Fig. 1C), and by shifting the gradient G_2 to the end of the second δ delay (shown in Fig. 1C by broken lines). (C) Spectrum obtained with the pulse sequence of Fig. 1A after insertion of a ^{15}N double filter before the 90°(^{1}H) pulse (DF in Fig. 1A).

the one of Fig. 1A, since it employs a difference between water magnetization and protein proton magnetization that is nearly twice as large. However, since the scheme requires that the amide protons should not be saturated, artifacts cannot be suppressed simply with a ^{15}N filter.

We further investigated an experiment in use for measurements of proton exchange and hydration in ^{13}C,^{15}N-labeled molecules that is based on the application of selective pulses on the water resonance (Fig. 1C) (*34*). In this scheme, radiation damping is effective during the delay δ after the refocusing of the water magnetization by the gradient G_2 and, for odd scans (scheme I), also during the mixing time following the gradient G_3, τ_m. The delay δ is rather short and the resulting radiation damping is represented as a truncated sech(t/τ_r) pulse of appropriate phase (x or $-x$). Since for odd scans the water magnetization at the start of the mixing time τ_m is antiparallel to the magnetic field, the phase of the water magnetization and hence of the radiation damping effect is nearly random (*38*). In our hands, even a standard test with water presaturation showed artifacts in experiments at 750 MHz. We then decreased the power and changed the shape of the selective water flip-back pulse in the {^{15}N,^{1}H}-HSQC pulse sequence (see Materials and Methods) when compared to the original scheme (*34*). The water–protein NOE spectrum obtained using this slightly modified pulse sequence (Fig. 4D) still contains apparent artifacts, since peaks are observed for some of the buried amide protons (compare with Fig. 4B). We did not investigate in detail the origin of all the artifacts obtained with this pulse sequence, but peaks originating from radiation damping could be reduced by keeping the solvent defocused during the delays δ and the mixing time τ_m. This was achieved by

applying a weak field gradient during the entire mixing time and shifting the refocusing gradient G_2 as close to the last selective 90° pulse as possible (Fig. 1C). Spectra obtained using the original experiment and the modified pulse sequence, respectively (Figs. 6A and 6B), demonstrate partial suppression of the artifacts by the modifications indicated by the dashed lines in Fig. 1C. Nevertheless, the suppression of the artifacts seems to be incomplete, as implied by a comparison with the spectrum of Fig. 6C, which was obtained with the pulse sequence of Fig. 1A after insertion of a ^{15}N double filter just before the 90°(^{1}H) pulse (dashed square in Fig. 1A).

Overall, considering that we investigated only three of the numerous pulse sequences that have been proposed for hydration studies and that the artifacts discussed here depend on the field strength B_0, we prefer not to propose a unique pulse sequence that would perform best. Otherwise the message seems clear: when working at high magnetic field strength B_0 one must keep in mind collective solvent effects when studying specific hydration by NMR.

CONCLUSIONS

In spite of its small magnitude (maximum strength 15–30 Hz) the radiation damping field may disturb nuclei resonating as much as 2 to 3 kHz away from the solvent signal. The amplitude of such disturbances can be of the order of 1% of the equilibrium nuclear magnetization and the corresponding signals may be visible, for example, when using difference techniques in studies of solvent–solute NOEs and exchange measurements. The absence of signals in the commonly used difference experiment with presaturation of the solvent signal before the start of the exchange experiment (e.g., Refs. *28, 51, 52*) is no guarantee for the absence of artifacts, since it eliminates radiation damping and the solvent demagnetizing field along with the artifacts arising from them. Pulse sequences for hydration measurements are very sensitive to small details in their implementation, such as short delays and positioning of gradient pulses, as well as to hardware parameters, such as the probe tuning and the time constant of the field–frequency lock system. To minimize artifacts in the spectra, extensive, time-consuming test procedures are required each time before collecting data. This is especially important when porting a pulse sequence to a higher-field spectrometer, where radiation damping and demagnetizing field effects are intrinsically stronger.

In general, the test procedures should include a cancellation test for the relay step, a difference test with presaturation of the solvent signal, and either an experiment with a very short mixing time (<5 ms) or the recording of buildup curves of the solvent–protein NOEs. Careful investigation of the NOE buildup for small time increments (~100 μs) can also be useful for testing such pulse sequences. The demagnetizing field effect can be a source of ''dispersive-

like'' subtraction artifacts. These artifacts can usually be suppressed by proper modification of the pulse sequence. In some cases water flip-back pulses may have to be sacrificed for the sake of data reliability. The deuterium field–frequency lock system can usually not fully compensate for the influence of the demagnetizing field, both since it has typically a rather long response time for optimal stability (see Fig. 3B) and because the deuterium signal is not sensitive to the transverse component of the proton demagnetizing field.

ACKNOWLEDGMENTS

REFERENCES

1. N. Bloembergen and R. V. Pound, Radiation damping in magnetic resonance experiments, *Phys. Rev.* **93,** 8–12 (1954).

2. W. S. Warren, S. L. Hammes, and J. L. Bates, Dynamics of radiation damping in nuclear magnetic resonance, *J. Chem. Phys.* **91,** 5895–5904 (1989).

3. M. Guéron, P. Plateau, and M. Decorps, Solvent signal suppression in NMR, *Prog. NMR Spectrosc.* **23,** 135–209 (1991).

4. P. Broekaert and J. Jeener, Suppression of radiation damping in NMR in liquids by active electronic feedback, *J. Magn. Reson. A* **113,** 60–64 (1995).

5. A. Louis-Joseph, D. Abergel, and J.-Y. Lallemand, Neutralization of radiation damping by selective feedback on 400 MHz NMR spectrometer, *J. Biomol. NMR* **5,** 212–216 (1995).

6. C. Anklin, M. Rindlisbacher, G. Otting, and F. H. Laukien, A probehead with switchable quality factor. Suppression of radiation damping, *J. Magn. Reson. B* **106,** 199–201 (1995).

7. W. C. Dickinson, The time average magnetic field at the nucleus in nuclear magnetic resonance experiments, *Phys. Rev.* **81,** 717–731 (1951).

8. J. Jeener, A. Vlassenbroek, and P. Broekaert, Unified derivation of the dipolar field and relaxation terms in the Bloch–Redfield equations of liquid NMR, *J. Chem. Phys.* **103,** 1309–1332 (1995).

9. H. T. Edzes, The nuclear magnetization as the origin of transient changes in the magnetic field in pulsed NMR experiments, *J. Magn. Reson.* **86,** 293–303 (1990).

10. G. Deville, M. Bernier, and J. M. Delrieux, NMR multiple echoes observed in solid ^{3}He, *Phys. Rev. B* **19,** 5666–5688 (1979).

11. D. Einzel, G. Eska, Y. Hirayoshi, T. Kopp, and P. Wölfle, Multiple spin echoes in a normal Fermi liquid, *Phys. Rev. Lett.* **53,** 2312–2315 (1984).

12. R. Bowtell, R. M. Bowley, and P. Glover, Multiple spin echoes in liquids in a high magnetic field, *J. Magn. Reson.* **88,** 643–651 (1990).

13. A. S. Bedford, R. Bowtell, and R. M. Bowley, Multiple spin echoes in multicomponent liquids, *J. Magn. Reson.* **93,** 516–532 (1991).

14. H. Körber, E. Dormann, and G. Eska, Multiple spin echoes for protons in water, *J. Magn. Reson.* **93,** 589–595 (1991).

15. M. A. McCoy and W. S. Warren, Three-quantum nuclear magnetic resonance spectroscopy of liquid water: Intermolecular multiple-quantum coherence generated by spin-cavity coupling, *J. Chem. Phys.* **93,** 858–859 (1990).

16. Q. He, W. Richter, S. Vathyam, and W. S. Warren, Intermolecular multiple-quantum coherences and cross correlations in solution nuclear magnetic resonance, *J. Chem. Phys.* **98,** 6779–6800 (1993).

17. W. S. Warren, W. Richter, A. H. Andreotti, and B. T. Farmer II, Generation of impossible cross-peaks between bulk water and biomolecules in solution NMR, *Science* **262,** 2005–2009 (1993).

18. D. Abergel, M. A. Delsuc, and J.-Y. Lallemand, Comment on: Is multiple quantum nuclear magnetic resonance spectroscopy of liquid water real? *J. Chem. Phys.* **96,** 1657–1658 (1992).

19. W. S. Warren, Q. He, M. A. McCoy, and F. C. Spano, Reply to the comment on: Is multiple quantum nuclear magnetic resonance spectroscopy of liquid water real? *J. Chem. Phys.* **96,** 1659–1660 (1992).

20. A. Vlassenbroek, J. Jeener, and P. Broekaert, Macroscopic and microscopic fields in high-resolution liquid NMR, *J. Magn. Reson. A* **118,** 234–246 (1996).

21. M. H. Levitt, Demagnetization field effects in two-dimensional solution NMR, *Concepts Magn. Reson.* **8,** 77–103 (1995).

22. R. Bowtell, Indirect detection via the dipolar demagnetizing field, *J. Magn. Reson.* **100,** 1–17 (1992).

23. S. Vathyam, S. Lee, and W. S. Warren, Homogeneous NMR spectra in inhomogeneous fields, *Science* **272,** 92–96 (1996).

24. P. Robyr and R. Bowtell, Measuring diffusion in liquids with a single gradient pulse, *J. Magn. Reson. A* **121,** 206–208 (1996).

25. P. C. M. Van Zijl, M. O. Johnson, S. Mori, and R. E. Hurd, Magic-angle-gradient double-quantum-filtered COSY, *J. Magn. Reson. A* **113,** 265–270 (1995).

26. D. L. Mattiello, W. S. Warren, L. Mueller, and B. T. Farmer II, Minimizing the water resonance in biological NMR: Characterization and suppression of intermolecular dipolar interactions by multiple-axis gradients, *J. Am. Chem. Soc.* **118,** 3253–3261 (1996).

27. G. M. Clore, A. Bax, J. G. Omichinski, and A. M. Gronenborn, Localization of bound water in the solution structure of a complex of the erythroid transcription factor GATA-1 with DNA, *Structure* **2,** 89–94 (1994).

28. J. A. Ernst, R. T. Clubb, H.-X. Zhou, A. M. Gronenborn, and G. M. Clore, Demonstration of positionally disordered water within a protein hydrophobic cavity by NMR, *Science* **267,** 1813–1817 (1995).

29. G. Otting and K. Wüthrich, Studies of protein hydration in aqueous solution by direct NMR observation of individual protein-bound water molecules, *J. Am. Chem. Soc.* **111,** 1871–1875 (1989).

30. G. Otting, E. Liepinsh, and K. Wüthrich, Protein hydration in aqueous solution, *Science* **254,** 974–980 (1991).

31. E. Liepinsh, G. Otting, and K. Wüthrich, NMR observation of individual molecules of hydration water bound to DNA duplexes: Direct evidence for a spine of hydration water present in aqueous solution, *Nucl. Acids Res.* **20,** 6549–6553 (1992).

32. Y. Q. Qian, G. Otting, and K. Wüthrich, NMR detection of hydration water in the intermolecular interface of a protein-DNA complex, *J. Am. Chem. Soc.* **115,** 1189–1190 (1993).

33. R. W. Kriwacki, R. B. Hill, J. M. Flanagan, J. P. Caradonna, and J. H. Prestegard, New NMR methods for the characterization of bound water in macromolecules, *J. Am. Chem. Soc.* **115,** 8907–8911 (1993).

34. S. Grzesiek and A. Bax, Measurement of amide proton exchange rates and NOEs with water in ^{13}C/^{15}N-enriched calcineurin B, *J. Biomol. NMR* **3,** 627–638 (1993).

35. P. X. Qi, J. L. Urbauer, E. J. Fuentes, M. F. Leopold, and A. J. Wand, Structural water in oxidized and reduced horse heart cytochrome c, *Nature Struct. Biol.* **1,** 378–381 (1994).

36. S. Mori, M. O. Johnson, J. M. Berg, and P. C. M. Van Zijl, Water exchange filter (WEX filter) for nuclear magnetic resonance studies of macromolecules, *J. Am. Chem. Soc.* **116,** 11982–11984 (1994).

37. V. Dötsch and G. Wider, Exchange rates of internal water molecules in proteins measured using pulsed field gradients, *J. Am. Chem. Soc.* **117,** 6064–6070 (1995).

38. G. Otting and E. Liepinsh, Selective excitation of intense solvent signals in the presence of radiation damping, *J. Biomol. NMR* **5,** 420–426 (1995).

39. C. Dalvit and U. Hommel, New pulsed field gradient NMR experiments for the detection of bound water in proteins, *J. Biomol. NMR* **5,** 306–310 (1995).

40. G. Wider, R. Riek, and K. Wüthrich, Diffusion filters for separation of solvent–protein and protein–protein nuclear Overhauser effects (HYDRA), *J. Am. Chem. Soc.* **118,** 11629–11634 (1996).

41. S. Mori, J. M. Berg, and P. C. M. Van Zijl, Separation of intramolecular NOE and exchange peaks in water exchange spectroscopy using spin-echo filters, *J. Biomol. NMR* **7,** 77–82 (1996).

42. S. Grzesiek, A. Bax, L. K. Nicholson, T. Yamazaki, P. Wingfield, S. J. Stahl, C. J. Eyermann, D. A. Torchia, C. N. Hodge, P. Y. S. Lam, P. K. Jadhav, and C.-H. Chang, NMR evidence for the displacement of a conserved interior water molecule in HIV protease by a non-peptide cyclic urea-based inhibitor, *J. Am. Chem. Soc.* **116,** 1681–1682 (1994).

43. S. Bloom, Effects of radiation damping on spin dynamics, *J. Appl. Phys.* **28,** 800–805 (1957).

44. A. Vlassenbroek, J. Jeener, and P. Broekaert, Radiation damping in high resolution liquid NMR: A simulation study, *J. Chem. Phys.* **103,** 5886–5897 (1995).

45. B. Lix, F. D. Sönnichsen, and B. D. Sykes, The role of transient changes in sample susceptibility in causing apparent multiple-

quantum peaks in HOESY spectra, *J. Magn. Reson. A* **121,** 83–87 (1996).

46. X. Mao and C. Ye, Line shapes of strongly radiation-damped nuclear magnetic resonance signals, *J. Chem. Phys.* **99,** 7455–7462 (1993).

47. G. Otting and K. Wüthrich, Heteronuclear filters in two-dimensional [^{1}H, ^{1}H]-NMR spectroscopy: Combined use with isotope labelling for studies of macromolecular conformation and intermolecular interactions, *Q. Rev. Biophys.* **23,** 39–96 (1990).

48. M. Ikura and A. Bax, Isotope-filtered 2D NMR of protein–peptide complex: Study of a skeletal muscle myosin light chain kinase fragment bound to calmodulin, *J. Am. Chem. Soc.* **114,** 2433–2440 (1992).

49. P. Broekaert, A. Vlassenbroek, J. Jeener, G. Lippens, and J.-M. Wieruszeski, Observation and selective suppression of the dipolar-field effects in 2D NMR in liquids in homogeneous fields, *J. Magn. Reson. A* **120,** 97–104 (1996).

50. M. G. Kubinec, A. S. Culf, H. Cho, D. C. Lee, J. Burkham, H. Morimoto, P. G. Williams, and D. E. Wemmer, Applications of tritium NMR to macromolecules: A study of two nucleic acid molecules, *J. Biomol. NMR* **7,** 236–246 (1996).

51. B. W. Matthews, A. G. Morton, and F. W. Dahlquist, Use of NMR to detect water within nonpolar protein cavities, *Science* **270,** 1847–1848 (1995).

52. J. A. Ernst, R. T. Clubb, H.-X. Zhou, A. M. Gronenborn, and G. M. Clore, Use of NMR to detect water within nonpolar protein cavities: Response, *Science* **270,** 1848–1849 (1995).

53. L. E. Kay, P. Keifer, and T. Saarinen, Pure absorption gradient enhanced heteronuclear single quantum correlation spectroscopy with improved sensitivity, *J. Am. Chem. Soc.* **114,** 10663–10665 (1992).

54. O. Zhang, L. E. Kay, J. P. Oliver, and J. D. Forman-Kay, Backbone ^{1}H and ^{15}N resonance assignments of the N-terminal SH3 domain of drk in folded and unfolded states using enhanced-sensitivity pulsed field gradient NMR techniques, *J. Biomol. NMR* **4,** 845–858 (1994).